Wiley
Advances in Civil Engineering
Volume 2025, Article ID 9530970, 20 pages
https://doi.org/10.1155/adce/9530970

WILEY

Research Article

Novel Mangrove-Guard Baffles for Rock Avalanche Protection: Numerical Analysis

Xin-Po Sun,[1,2] **Shi-Jie Luo**,[1,2] **Chun-Ying Wang**,[1,2] **Lu Zheng**,[3] **Wan-Hui Su**,[1,2] **Xin-Yi Wang**,[2,4] **and Zhe-Yuan Jiang**[2,5]

[1]*College of Civil Engineering, Sichuan University of Science and Engineering, Zigong 643000, China*
[2]*SUSE-BZ Geoenvironmental Engineering Joint Laboratory, Sichuan University of Science and Engineering, Zigong 643000, China*
[3]*College of Civil Engineering, Fuzhou University, Fuzhou 350108, China*
[4]*School of Design, Hong Kong Polytechnic University, Hong Kong 999077, China*
[5]*Jiangsu Key Laboratory of Low Carbon and Sustainable Geotechnical Engineering, Institute of Geotechnical Engineering, Southeast University, Nanjing 210096, China*

Correspondence should be addressed to Xin-Yi Wang; 22047408g@connect.polyu.hk and Zhe-Yuan Jiang; jiangzheyuan@seu.edu.cn

Received 3 December 2024; Revised 10 June 2025; Accepted 11 July 2025

Academic Editor: Jian Ji

Rock avalanches pose significant threats to infrastructure due to their high kinetic energy. Baffle structure serves as an effective engineering solution for mitigating rock avalanche hazards. In this study, a new mangrove guard baffle (MGB) was proposed by combining traditional baffle (TB) designs with the prop root structure of mangroves. Using EDEM software, simulations were conducted to analyze the impact of baffle type and particle size on the movement velocity, deposition, impact force, and kinetic energy of rock avalanches. The results indicated that the process of rock avalanche impact on a baffle could be divided into four stages: initiation, acceleration, impact, and static deposition. The maximum average front velocity obtained by the rock avalanche in the acceleration phase was about 4.5 m/s, and the maximum average tail velocity was about 3 m/s. In addition, the MGB created a larger dead zone and reduced the deposition area. Compared to the STB, under the SMGB, the deposition areas of M1–M4 decreased by 17.9%, 12.7%, 17.1%, and 16%, respectively. MGB demonstrated superior impact force dissipation. When the number of baffle rows was three, the impact force dissipation rate of SMGB on M4 reached 99%. Compared to TBs, the momentum of the rock avalanche was reduced by 1%–3%. Considering the economic benefits and protection performance, the arrangement of two rows of baffles could be the best solution. These findings provided insights into the design of baffle structures against rock avalanches.

Keywords: economic benefits; kinetic energy reduction; mangrove-guard baffles; particle deposition; rock avalanches

1. Introduction

Rock avalanches are extremely rapid, massive, flow-like movements of fragmented rock from a large rock slide or rockfalls [1–3]. Rock avalanche exhibits robust destructive power and extremely high mobility; thus, rock avalanches can cause huge property losses and casualties [4–6]. As a result, researchers have increasingly addressed disaster prevention design.

In practical engineering, to reduce the damage caused by rock avalanches, scientists have proposed various protective structures. These structures can be divided into either closed or open. The closed structures, like check dams [7, 8], open structures like flexible barriers [9], slit dams [10], and baffles [11, 12]. However, check dams and slit dams are costly and prone to blockage, and difficult to clean [8]. Flexible barriers are mainly used for debris flow prevention [13]. In recent years,

arrays of baffle have been used to counter rock avalanches due to their low cost, high strength, and excellent blocking performance [14–16]. Baffles are usually set downstream of the rock avalanche flow path, which can effectively disrupt the flow conditions of the rock avalanche, dissipating the impact force and energy of the rock avalanche. The typical application of baffles in actual engineering projects in China is shown in Supporting Information: Table A1. Square and cylindrical baffles are widely used in practical engineering.

Many scholars have conducted extensive research on the effect of baffles in reducing flow velocity or impact force. These studies mainly include conventional gravity model experiments and numerical simulations. Ng et al. [11] used a flume model experiment to study the effects of square baffle (SB) array layout parameters on the flow state of rock avalanches, finding that three rows of baffles can reduce jumping by 65% and frontal velocity by 57%. Building on this, Ng et al. [16] used small-scale model tests to investigate the interaction mechanisms between dry granular flow and multirow SB arrays, providing references for the design of multirow baffle structures. Wang et al. [17] proposed an arc-shaped baffle (ASB) structure and validated its effectiveness through small-scale model tests. Scheidl et al. [18] studied the impact characteristics of granular debris flows based on small-scale physical experimental models, discovering that the peak pressure of granular debris flows is related to stress anisotropy, volume density, and the height of rise during impact. Choi et al. [19], Law et al. [20], and Bi et al. [21] used the discrete element method (DEM) model to investigate the interaction mechanisms between SB arrays and rock avalanches, analyzing the impact of baffle array configurations on the impact force of granular flow. Huang et al. [22] examined the effect of rock avalanche particle size on the performance of square and triangular baffles through DEM simulation, showing that SBs perform better than triangular ones.

However, previous studies mainly focused on the square and cylindrical baffles. The huge impact and destructive force of rapid rock avalanches often reduce the interception efficiency of traditional baffles (TBs), or even destroy them. Therefore, optimizing the baffle structure to improve its disaster resistance is a key issue. Bi et al. [23] optimized the baffle-net structure, finding that the energy dissipation rate of optimized structure reached 91%, an increase of nearly 24% over the original structure. Wang et al. [15] used the discrete element numerical simulation method to analyze the energy dissipation effect on rock avalanches of baffles with different shapes, and found that the arc structure has the best energy consumption effect. Choi [24] conducted a flume test and found that compared with the vertical-shaped barrier, the arc-shaped barrier can reduce the rising height caused by the impact of the particle flow by 17% and prolong the impact duration by 15%. Bi et al. [25] optimized the design of the TBs, and numerical research shows that optimized baffles can reduce the particle mass behind the baffle by 2–3 times. Nevertheless, the effects of optimization on rock avalanche deposition, impact force dissipation, and energy dissipation are not well quantified. Furthermore, most studies have focused on the macro-level interactions between the flow-baffle, while the micromechanism has barely been clarified.

Additionally, particle size significantly affects the stress transmission mechanism within a fluid. As particle size increases, the stress transmission shifts from being contact-dominated to collision-dominated [26–28]. This means that when the particles are smaller, stress is primarily transmitted through direct contact between them. However, when the particles are larger, collision and rebound between the particles become the main mode of stress transfer. In confined spaces, larger particles are more likely to cause local blockage. These blockages not only alter the interactions between particles but also affect the fluid velocity, disrupting the normal flow pattern. The blockage effect of the particles may lead to localized increases in fluid pressure or energy dissipation, significantly alter the kinematics and impact force of the fluid [29].

On the other hand, the particle size distribution affects the deposition behavior of rock avalanches, leading to the particle segregation effect [30]. The particle segregation effect shows that, under specific flow dynamic conditions, smaller particles tend to deposit at the bottom, while larger particles accumulate at the top. This variation in particle size distribution influences the internal movement of particles. It also enhances the climbing ability of larger particles, increasing the impact force and disaster potential of rock avalanches. By studying the behavior of different particle sizes, we explore the role of the particle segregation effect in fluid dynamics. This helps reveal the mechanical characteristics and disaster risk mechanisms during rock avalanche impacts on baffles. Therefore, particle size is a critical consideration in baffle design.

In addition to particle size, other material properties also significantly affect the behavior of rock avalanches. Recent studies have shown that the shape of particles plays a crucial role in determining flow mobility and stress distribution within the granular mass. Irregularly shaped particles exhibit higher interlocking effects, leading to greater resistance to movement, while more rounded particles tend to enhance flow mobility due to reduced friction. Moreover, the size-shape correlation has been found to influence the deposition and impact characteristics of rock avalanches, affecting their overall kinematics and interaction with barriers [31]. These factors are essential in understanding the impact force exerted by rock avalanches on protective structures, as highlighted by Li et al. [32], who proposed a semi-empirical impact force model to account for irregular rockfall interactions with granular layers.

Furthermore, ice content is another critical factor influencing rock avalanche behavior, especially in cold regions. The presence of ice can alter the cohesion between particles, significantly modifying their impact force and deposition patterns. Wang et al. [33] conducted physical and numerical modeling to analyze the effect of ice content on rock-ice avalanche interactions with rigid barriers, demonstrating that higher ice content increases the runout distance and modifies impact forces. Similarly, Fang et al. [34] provided new insights into the dynamic impact mechanisms between geophysical flows and rigid barriers, emphasizing the importance of considering material properties when designing protective structures. Since this

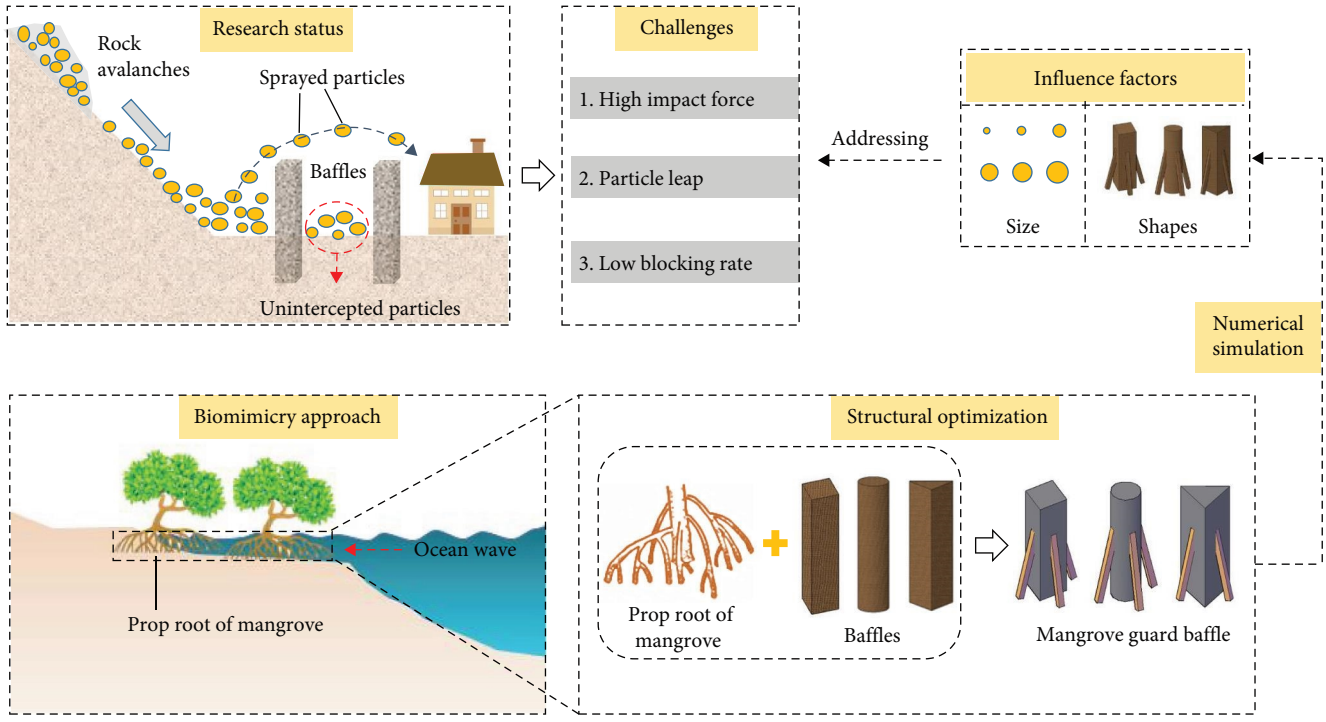

FIGURE 1: The design idea of mangrove guard baffle.

study does not incorporate the effects of particle shape, ice content, or size-shape correlation, future research should consider these factors to provide a more comprehensive understanding of rock avalanche dynamics and their implications for baffle design.

In summary, this paper proposed a mangrove guard baffle (MGB) based on the design concept of Bi et al. [25] and the principle of similar function and structure between the baffle and mangrove. The study aimed to address the issues of low interception efficiency and severe particle leaps observed in current baffle research. The research steps are shown in Figure 1. The study specifically examined the movement behavior, deposition morphology, impact force dissipation, and energy dissipation of rock avalanche particles of four different sizes under various baffle conditions. Finally, the interception mechanism of the MGB against rock avalanches and its economic benefits were discussed.

2. Methodologies

2.1. DEM. In this study, the commercial software EDEM was used to simulate the interaction between rock avalanches and arrays of baffle, and the effectiveness of numerical tests has been validated [35, 36]. EDEM is a particle material simulation software based on the DEM, which enables the simulation and analysis of particle handling processes in industrial production and related manufacturing equipment. The user can set the properties of each particle (mass, velocity, etc.) and information about the force applied to the particles. The particle factory technology of EDEM provides a unique and efficient method for generating particle assemblies that can well simulate the movement of landslide debris flows. The mathematical model selected is Hertz–Mindlin (no slip) model, which is an elastic-plastic model and the default model used in EDEM. It is known for its accuracy and efficiency in force calculations and has been widely used to simulate particle flow [35, 37].

2.2. Flume Model and Calculation Scheme. The numerical model used in this study is shown in Figure 2. The model is mainly composed of four parts: source box, chute, deposition platform, and arrays of baffle (Figure 2a). The size of the source box is $400 \times 300 \times 400$ mm by length, width, and height, the chute is $4000 \times 300 \times 400$ mm. The slope angle is 35°, and the deposition platform is $2000 \times 2000 \times 400$ mm. The baffle structures used in this study are shown in Figure 2b, including STB, SMGB, CTB, CMGB, TTB, and TMGB. The complete list of symbols is presented in Table 1. To investigate the effect of particle size on rock avalanche movement, four types of graded particles were designed, as shown in Figure 2c. As shown in Figure 2d, the arrays of baffle in this paper adopt the structure of three rows of baffles, with the side length of 50 mm and the height (h) of 180 mm, which are placed in the downstream platform. As shown in Figure 2e, the retaining distance $L_d =$ 400 mm (the distance from the chute port to the first row of baffles), the baffle row spacing $S_r = 90$ mm, and the baffle column spacing is $S_c = 70$ mm. The measurement area is long enough in Z and Y directions to detect all particles passing through the measurement area during the simulation process.

2.3. Parameter Inversion. The particle size, shape, and input parameters of the particles play a key role in EDEM. The shape of the particles is generally spherical to approximate actual particles. The most important and difficult part is the influence of material parameters. While EDEM can model the bouncing, falling, sliding, and rolling of elementary particles, it is difficult

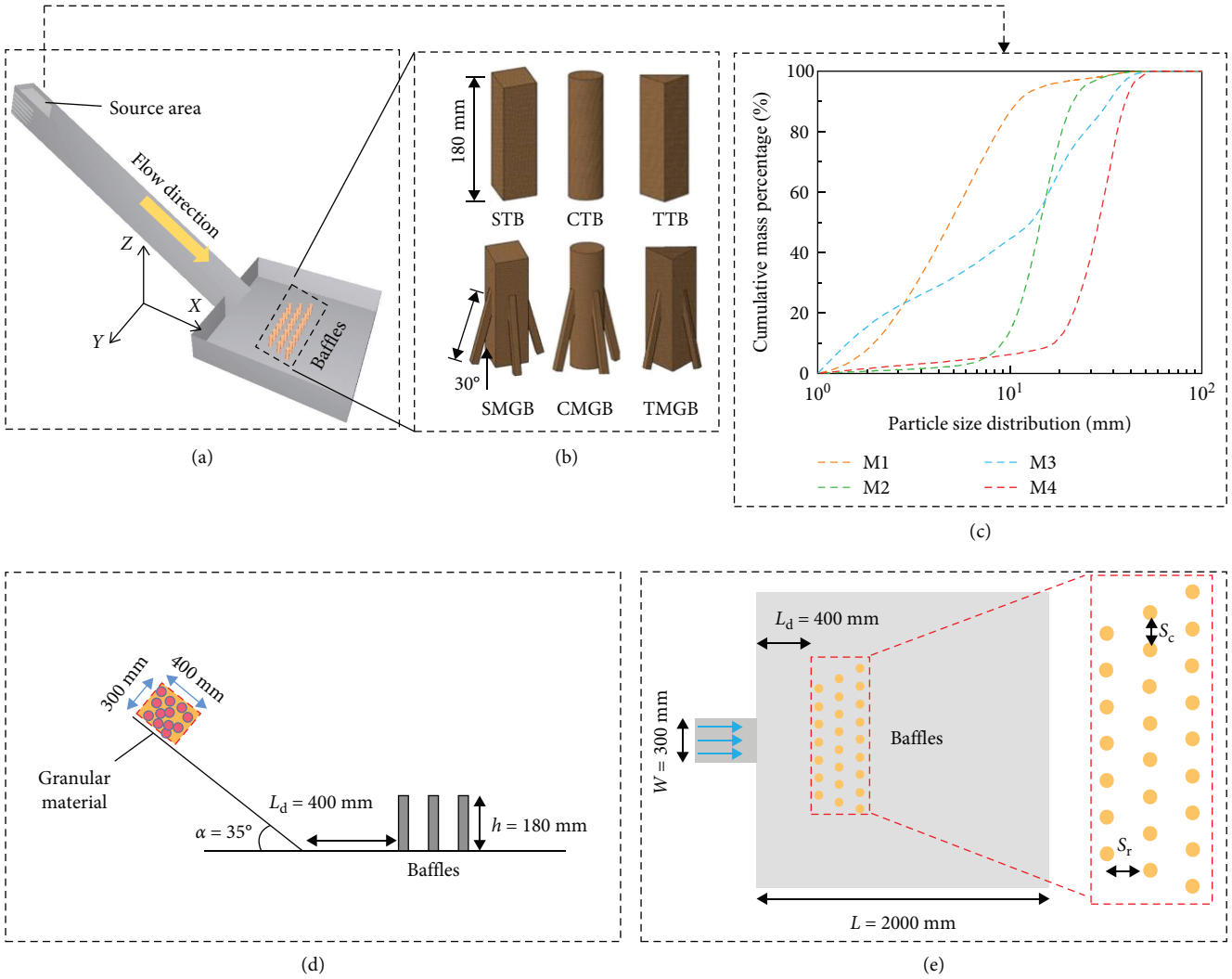

FIGURE 2: EDEM model of rock avalanches impact arrays of baffle: (a) numerical model, (b) baffles type, (c) particle size distribution, (d) side view of schematic, and (e) top view of numerical model.

to accurately determine and quantify some of the parameters associated with these motions. Therefore, in order to ensure that the established model is suitable for subsequent study, the model parameters need to be verified. There are generally two methods to determine the similarity of parameters used in simulated physical tests: (1) similar deposition shape and (2) similar impact force. In method (1), parameter inversion is performed by comparing the deposition morphology between the physical test and numerical simulation at different time steps. In method (2), parameter inversion is conducted by comparing the impact force between the physical test and numerical simulation. In this study, method (1) was used to obtain the final material parameters.

In this section, a small-scale physical test of a flume rock avalanche was conducted, and the final morphology of deposition between physical test and numerical simulations is shown in Supporting Information: Figure A1a,b. Then, based on the physical test, the morphology of deposition of the physical test and the numerical simulation at different time steps was compared. As shown in Supporting Information: Figure A1c,d, when $t = 1.56$ s, the rock avalanche attempted to cross the arrays of baffle, and the arrays of baffle began to block the debris. At $t = 1.92$ s, the rock avalanche moved to the sides under the action of the arrays of baffle. When $t = 4.0$ s, all rock avalanche particles had almost stopped moving, exhibiting a final deposition morphology. The results of numerical simulation in the Figure A1 showed good agreement with the physical test results.

Savage and Hutter [38] investigated the dynamics of particle flow using dimensionless expressions. Therefore, although there is a size effect in the source region, it is still possible to refer to their research methods and use dimensionless expressions to compare particle flows of different sizes. The dimensionless expression of motion time and velocity is as follows:

$$t^* = \frac{t}{\sqrt{L_0/g}}, \tag{1}$$

$$U^* = \frac{U}{\sqrt{gL_0}}, \tag{2}$$

Table 1: The list of symbols.

Abbreviation/symbol	Explanation
STB	Square traditional baffle
CTB	Cylinder traditional baffle
TTB	Triangular traditional baffle
SMGB	Square mangrove guard baffle
CMGB	Cylinder mangrove guard baffle
TMGB	Triangular mangrove guard baffle
M1, M2, M3, M4	Particle size distribution
α	Slope angle
L_d	The distance between the first row of the arrays of baffle and the chute port
h	The height of baffle
W	The width of chute
S_c	Baffle column spacing
S_r	Baffle row spacing
δ	Particle diameter
ρ_s	Particle density
G_S	The shear model of particle
υ_s	Particle poisson's ratio
ρ_0	Baffle (flume) density
G_0	The shear modulus of pile (flume)
υ_0	Baffle (flume) poisson' ratio
e_c	Coefficient of restitution
μ_1	Particle friction coefficient
μ_{r1}	Particle rolling friction coefficient
μ_0	Baffle (flume) friction coefficient
μ_{r0}	Baffle (flume) rolling friction coefficient
g	Gravitational acceleration
Δt	Time steps
t^*	Nondimensional travel time
U^*	Dimensionless form of travel velocity
VRR, v	Velocity reduction ratio
BR, n	Blockage ratio
IFDR, η	Impact force dissipation ratio
EDR, ε	Energy dissipation ratio

where the t^* is the dimensionless motion time, t is the standard form of time, U^* is the dimensionless form of motion velocity, U is the standard form of motion velocity, g is the acceleration of gravity, and L_0 is the particle length.

Supporting Information: Figure A2 shows the comparison between the laboratory rock avalanche movement data and the dimensionless velocity simulated by DEM in this study. It can be seen from Figure A2 that the velocity changes over time in both experiments followed the same trend, the maximum value of U^* was nearly identical, and the velocity curves were basically identical. However, there are differences between the simulation results and the experimental results when t^* ranges from 1.0 to 1.5, which may be due to the difference in particle shape between the simulation and the physical experiment. The collision between spherical particles in the numerical simulation further reduces the velocity of rock avalanches.

Table 2 summarizes the key material parameters obtained from the numerical experiments. As shown in Supporting Information: Figures A1 and A2, the simulation plan for this study is presented in Supporting Information: Table A2. The final deposition conditions and dimensionless velocity (U^*) from the simulation experiments are generally consistent with the results of the physical experiments. Given the good agreement between the numerical and experimental results, these parameters can be used for further study of granular avalanches.

3. Results and Analysis

3.1. Analysis of the Movement of Rock Avalanches With Different Baffles. Figure 3 illustrates the impact process and velocity changes of rock avalanches with a particle size of M1 as they impact the STB. As depicted in Figure 3a, at $t = 0$ s, particles gradually formed in the source area. Once all particles were formed, they remained in a static deposited state. At $t =$ 0.45 s, under the influence of gravity, the particles began to collapse, displaying a distinct stratified trend in velocity; particles at the forefront achieved higher velocity, while those at the rear, compressed by the mass above, had not yet begun to move and thus maintain lower velocity (Figure 3b). By $t = 1.2$ s, as shown in Figure 3c, all particles have started to move. At $t =$ 1.45 s, as the particles reached the platform, stratification occurred with some particles experiencing a bounce effect, impacting the baffles at higher velocity, while others, due to gravity and friction, flowed along the platform at lower velocity (Figure 3d). The baffles intercepted a significant volume of moving rock avalanche particles, leading to the formation of a deposition zone where particles at the rear encounter the previously formed deposition, causing them to disperse laterally along the original path, as shown in Figure 3e. Ultimately, by $t = 4.0$ s, under the combined effects of the baffles and the accumulating particles, all particles ceased moving and settled into a complete static deposition. The results suggested that the process of rock avalanche particles impacting the baffle can be divided into four stages: initiation, acceleration, impact, and static deposition.

The front velocity refers to the movement velocity of the leading edge of geological disasters, such as landslides and debris flows. By measuring and analyzing the front velocity, the development trend and potential hazards of the disaster can be assessed. Tail velocity refers to the movement velocity of the trailing edge of the disaster. The tail velocity helps in evaluating the duration of the disaster and the material transport volume [39]. The velocity calculation in this study is based on the Hertz–Mindlin (no slip) model, which determines particle motion through Newton's second law and contact force calculation [40]. The instantaneous velocity v_i of a particle i is given by:

$$m_i \frac{dv_i}{dt} = \sum F_{ij} + m_i g, \tag{3}$$

where m_i is the particle mass, F_{ij} represents all contact forces acting on particle i, and g is the gravitational acceleration. The front velocity v_{front} is defined as the average velocity of the particles at the leading edge, while the tail velocity v_{tail} is

Table 2: DEM input parameters.

Material parameters	Value	Contact parameters	Value
Particle diameter, δ (mm)	1–40	Coefficient of restitution	0.5
Particle density, ρ (kg/m^3)	2100	Particle friction coefficient, μ_1	0.8
Shear model of particle, G_S (GPa)	0.8	Particle rolling friction coefficient, μ_{r1}	0.15
Particle poisson's ratio, υ_0	0.25	Baffle (flume) friction coefficient, μ_0	0.453
Baffle (flume) density, ρ (kg/m^3)	7900	Baffle (flume) rolling friction coefficient, μ_{r0}	0.05
Shear modulus of baffle (flume), G_0 (GPa)	70	Gravitational acceleration, g (m/s^2)	9.81
Baffle (flume) poisson' ratio, υ_1	0.3	—	—

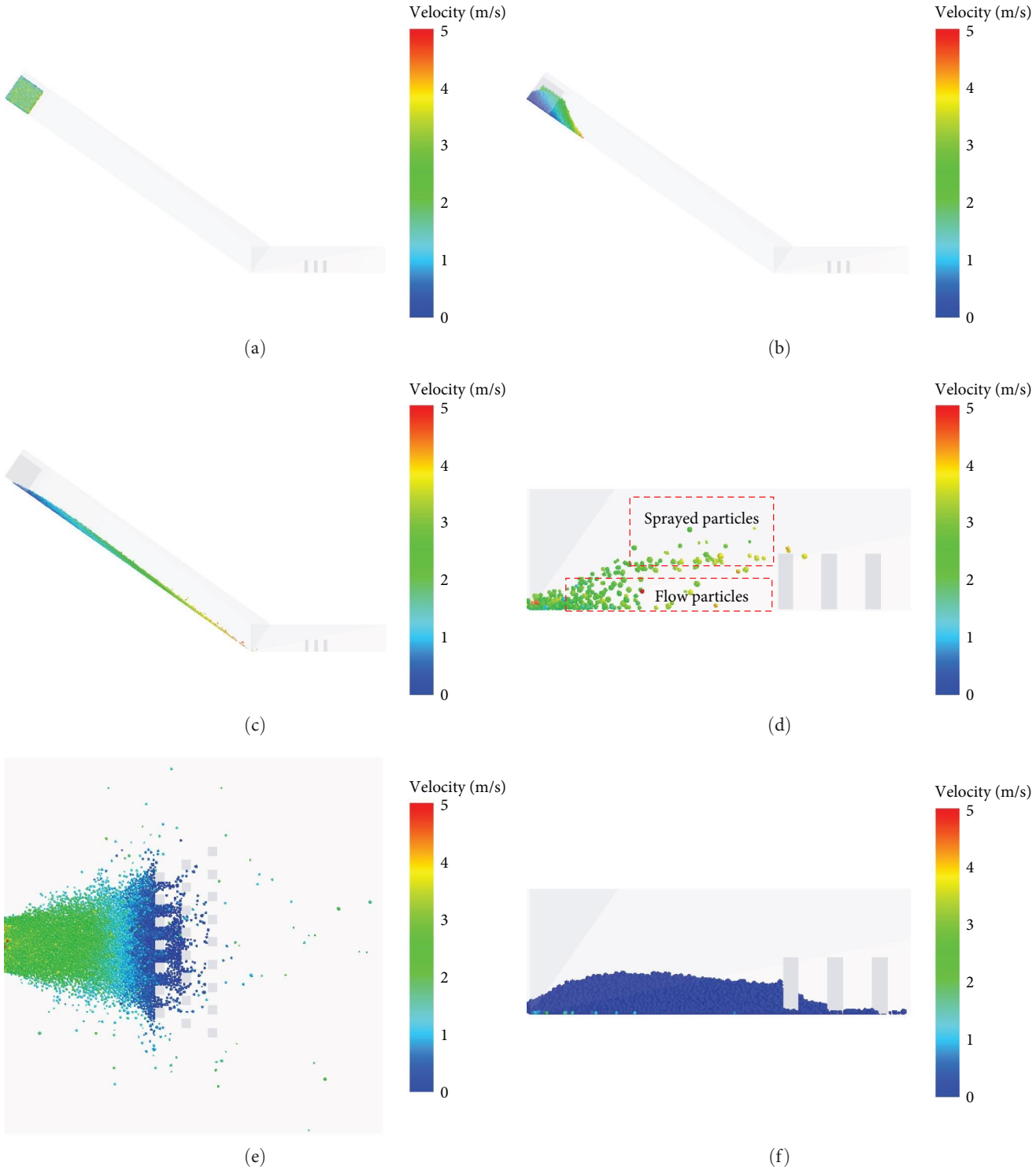

Figure 3: The moving processing of rock avalanches: (a) $t = 0$ s, (b) $t = 0.45$ s, (c) $t = 1.2$ s, (d) $t = 1.45$ s, (e) $t = 2.2$ s, and (f) $t = 4$ s.

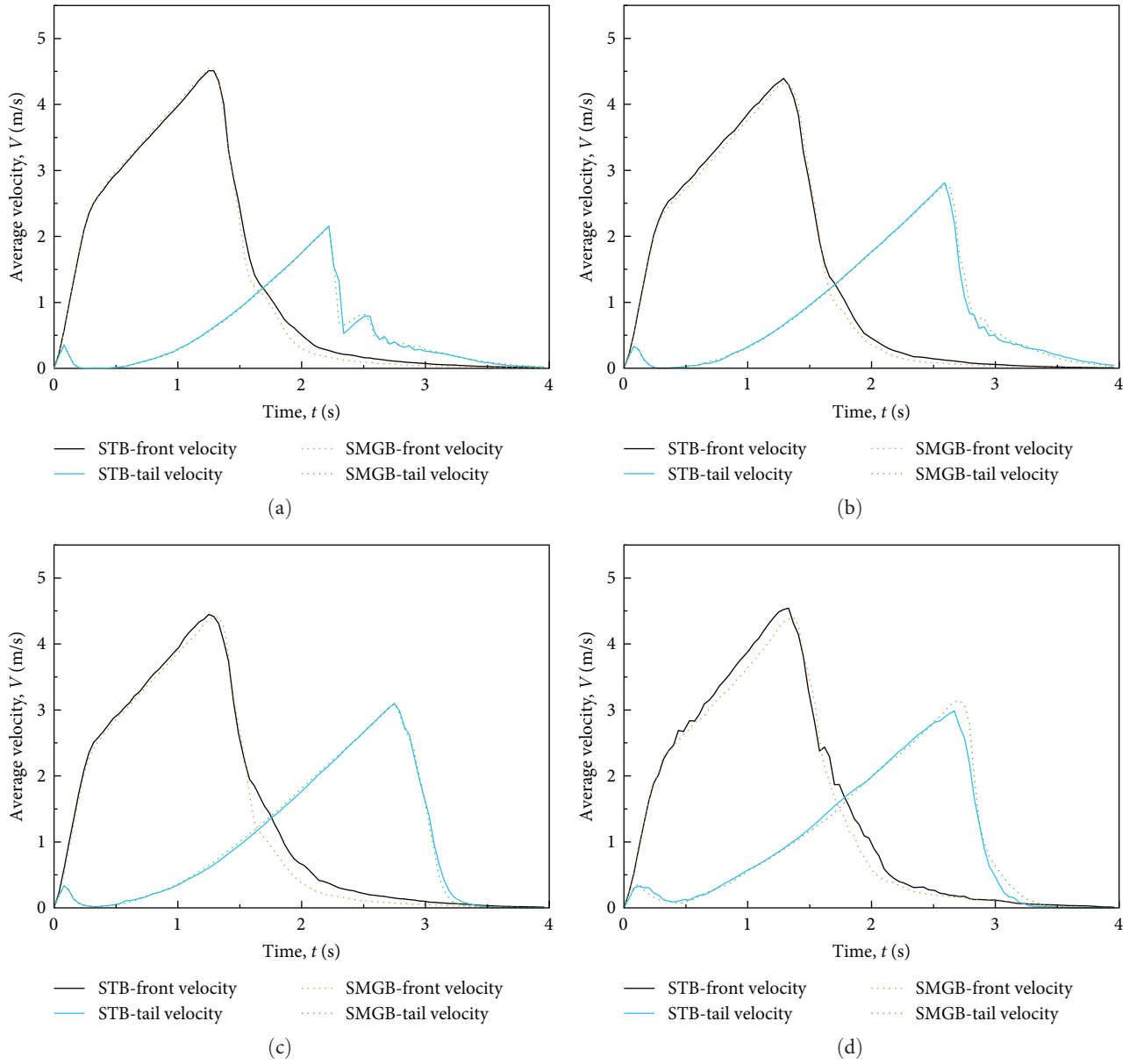

FIGURE 4: Front and tail velocity of rock avalanches with different size: (a) M1, (b) M2, (c) M3, and (d) M4.

the average velocity of the particles at the trailing edge [41] as follows:

$$v_{\text{front}} = \frac{1}{N_{\text{f}}} \sum_{i=1}^{N_{\text{f}}} |v_{\text{i}}|, \tag{4}$$

$$v_{\text{tail}} = \frac{1}{N_{\text{t}}} \sum_{i=1}^{N_{\text{t}}} |v_{\text{i}}|, \tag{5}$$

where N_{f} and N_{t} are the number of particles in the front and tail regions, respectively.

Figure 4 illustrates the front and tail velocity of rock avalanches of different sizes. As shown in Figure 4, as the particle size of rock avalanche increased, the peak velocity of front and tail increased. The front velocity of rock avalanches intercepted by two types of baffles initially followed the same trend, with peak velocity fluctuating around 4.5 m/s. This indicated that the velocity during the acceleration phase (before $t = 1.2$ s) was mainly determined by the material. At $t = 1.45$ s, the front velocity of the rock avalanches began to show differences due to the interception of the two types of baffles. With SMGB interception, the front velocity of the rock avalanches further decreases. All four sizes of rock avalanches exhibited the same phenomenon, indicating that SMGB had a certain effect in reducing the front velocity of the rock avalanches. It is important to note that due to the high front particle velocity during rock avalanches, some particles leaped over the baffle, resulting in a still high front velocity. In addition, tail velocity was slowed down due to the deposition of particles at the front, which were affected by interparticle friction, with the baffle having a minimal effect. Therefore, the MGB had a limited impact on reducing both the front and tail velocity.

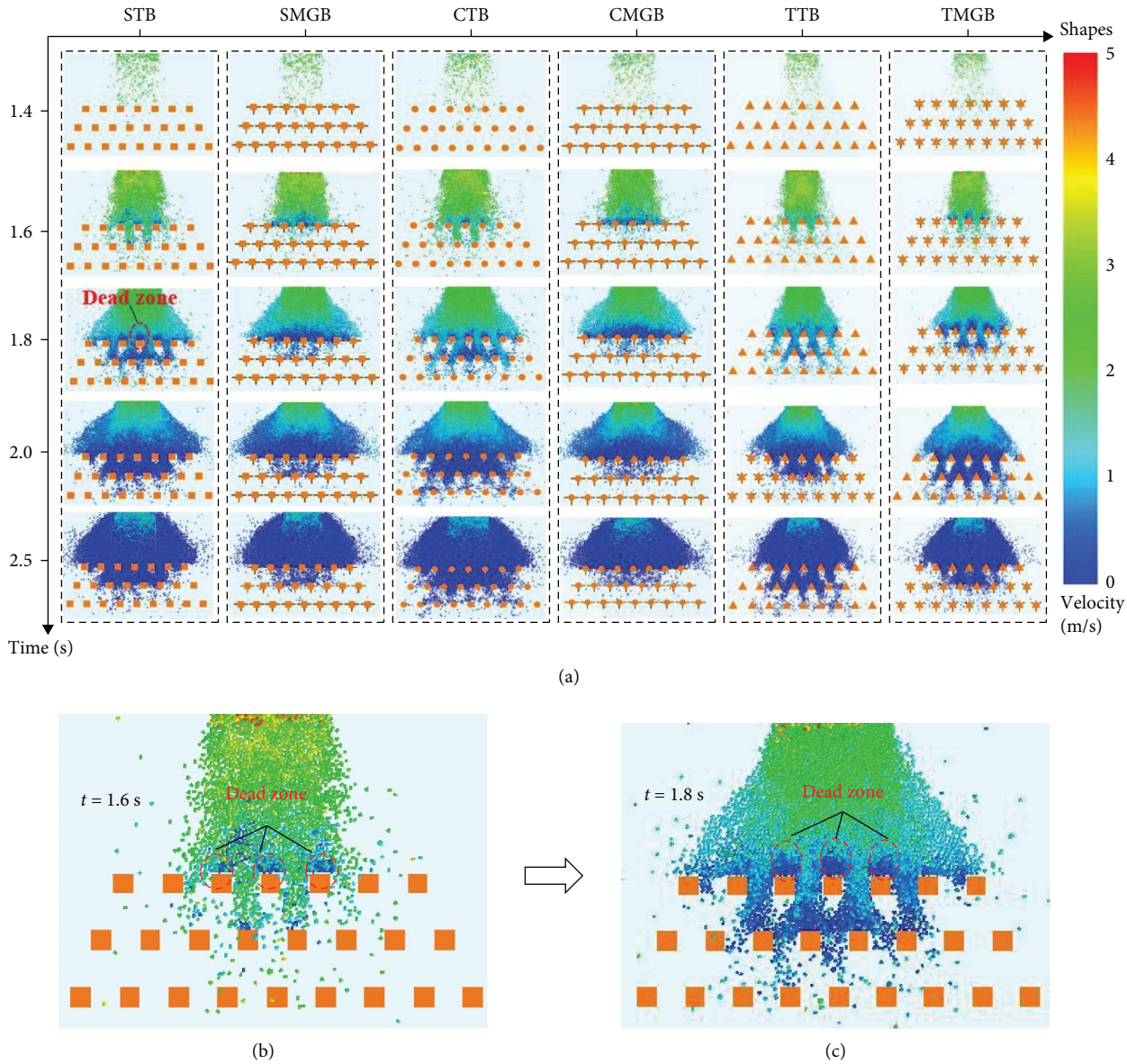

FIGURE 5: The process of rock avalanches deposition: (a) comparison of rock avalanche deposition morphology under different baffles interception, (b) the morphology of dead zone with STB at $t = 1.8$ s, and (c) the morphology of dead zone with SMGB at $t = 1.8$ s.

Notably, the tail velocity varied significantly with the size of rock avalanche. The peak tail velocity rises from 2 m/s to over 3 m/s. This indicates that as the size of the rock avalanche increases, both the intensity and duration of the disaster also increase.

3.2. Analysis of Rock Avalanches Deposition Form Under Different Arrays of Baffle. In the field of geological hazards, when the granular flow is impeded by barriers along its flow path, it may transition from a flowing state to a quasi-static state, forming a hydrodynamic dead zone [42, 43]. However, it should be noted that a dead zone primarily refers to the dynamic characteristics of the geological hazard process, rather than the final static deposit. The volume of dead zones is a critical factor in baffle design. Dead zones can affect the overall flow behavior of the rock avalanche particles, potentially causing localized erosion or deposition, thereby impacting the stability and functionality of the structure. Figure 5a illustrates the deposition process of rock avalanche particles and the changes in the dead zone from $t = 1.4$ to 2.5 s. It can be observed that due to the effect of the prop roots of the MGB, a larger dead zone was formed in front of the first row of baffles (Figure 5b, c). From a disaster prevention perspective, a larger dead zone indicates that more rock avalanche particles are intercepted and deposited by the baffles, reducing the number of particles that continue to flow downstream, thereby lowering the risk of impact and damage to downstream structures or facilities from rock avalanche particles.

To evaluate the blocking effect of different baffles on rock avalanche particles, a quantitative comparison of the resulting dead zones was conducted. The size of the dead zone R_d was quantified by the ratio of the volume of dead zone (V_d) to the total volume of the rock avalanche particles (V_t),

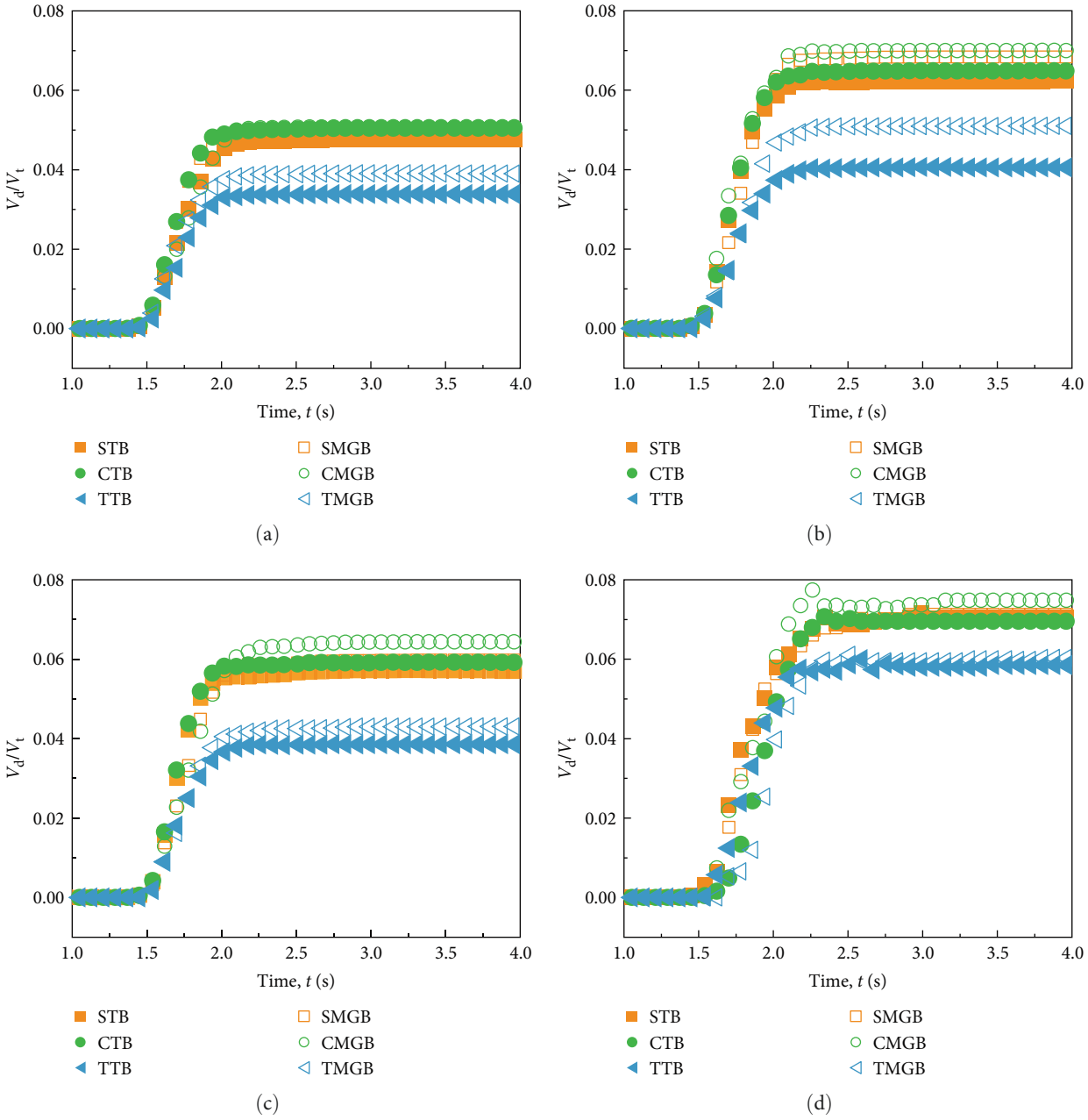

FIGURE 6: The change of dead zone: (a) M1, (b) M2, (c) M3, and (d) M4.

$$R_d = \frac{V_d}{V_t}, \tag{6}$$

$$V_d = \sum_{i=1}^{N} V_i,\ V_i \le V_{th}, \tag{7}$$

$$V_t = \sum_{i=1}^{N} V_i, \tag{8}$$

where V_i represents the volume of an individual particle, and N is the total number of particles that satisfy $V < V_{th}$. In granular flow studies, dead zones are typically identified using a velocity threshold method. A dead zone is defined as the region where particle velocity falls below a critical threshold V_{th}, typically set to 5%–10% of the maximum flow velocity [44] as follows:

$$V_{th} = \alpha\, V_{max},\ \alpha \in [0.05, 0.10], \tag{9}$$

$$V_d = \sum_{i=1}^{N} V_i,\ V_i \le V_{th}, \tag{10}$$

where V_{max} is the maximum particle velocity in the entire simulation, α is an empirical coefficient, commonly chosen between 0.05 and 0.10 [45].

As shown in Figure 6, the dead zone variation curve initially increased and then stabilized over time, indicating that the dead zone gradually formed and reached a certain volume as time

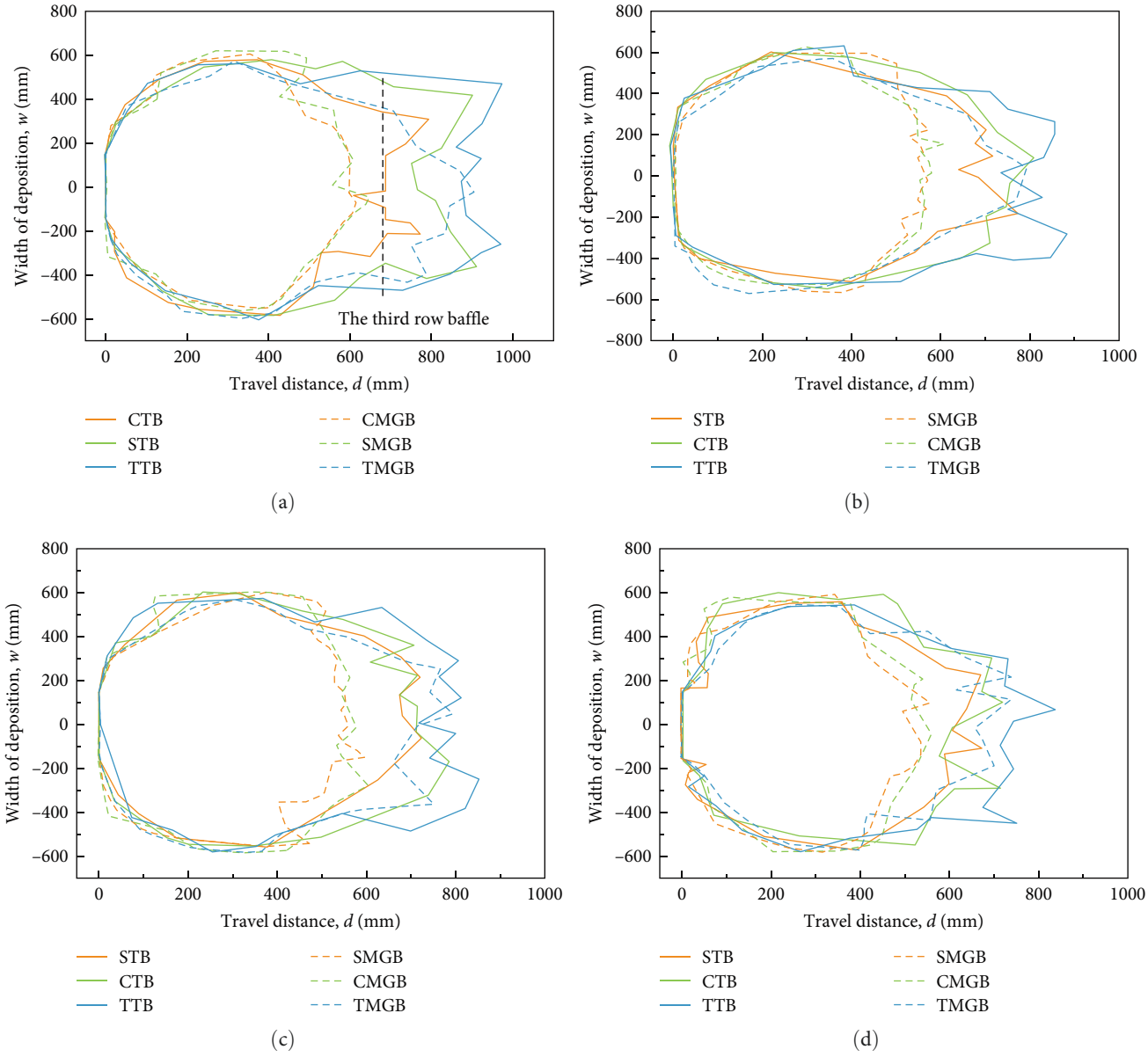

Figure 7: Influence of baffle type on rock avalanches deposition form: (a) M1, (b) M2, (c) M3, and (d) M4.

progressed. After a specific time threshold, no additional dead zone formation occurred, leading to an equilibrium state. Additionally, curves that rose quickly indicate that the dead zone formed more rapidly, meaning that the baffles effectively reduced particle velocity at an early stage, preventing further propagation of rock avalanche particles. For M1–M4, the CMGB had a relatively high dead zone volume ratio (R_d = 0.051, 0.070, 0.064, and 0.075), showing the best interception efficiency, which was more conducive to disaster prevention as it could intercept a greater number of particles. However, due to substantial accumulation of particles in front of the baffles, more frequent maintenance and clearing of the deposits were required. TTB had the lowest dead zone volume ratio among all baffles, and an excessively low dead zone ratio indicated a poorer blocking effect, allowing a large number of rock avalanche particles to flow downstream, increasing the risk of impact.

Overall, the effectiveness of a baffle depended not only on the final dead zone volume ratio (R_d) but also on the rate at which the dead zone formed and its steady-state behavior. An optimized baffle design should rapidly generate a sufficient dead zone to prevent excessive particle movement downstream while also considering maintenance challenges associated with excessive particle accumulation.

In order to study the effect of different baffles on the deposition morphology of rock avalanche particles, this research analyzed the static deposition morphology of rock avalanche particles with four different particle sizes impacting six types of baffles. The study calculated both the area of the deposition and the mass of the dispersed particles, aiming to provide a viable method to evaluate and compare the effectiveness of different baffle designs. As shown in Figure 7, there was a significant difference in the deposition morphology of rock avalanche

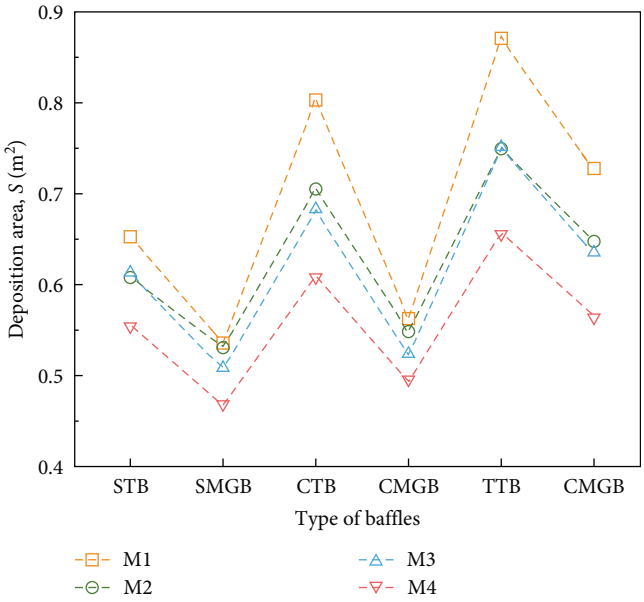

FIGURE 8: Deposition area of rock avalanches.

particles under different baffles. For rock avalanche particles ranging from M1 to M4, TB showed a larger deposition area compared to MGB. According to deposition morphology, this is because the particles intercepted by TB traveled further distances.

Figure 8 shows the trend of deposition area under different baffles. As the particle size of the rock avalanches increased, the area of the deposition morphology tended to decrease, with SMGB and CMGB showing smaller deposition areas for sizes M1–M4. When intercepted by SMGB, the deposition areas for M1–M4 were 0.536, 0.531, 0.507, and 0.467 m^2, respectively. In contrast, when blocked by STB, the deposition areas for M1–M4 were 0.65, 0.61, 0.61, and 0.56 m^2, respectively. Similarly, when intercepted by CMGB, the deposition areas for M1–M4 are 0.563, 0.548, 0.522, and 0.493 m^2, respectively. While blocked by CTB, the deposition areas for M1–M4 were 0.80, 0.71, 0.68, and 0.61 m^2, respectively.

As shown in Figure 9a, inorder to quantitatively analyze the extent of the rock avalanche hazard in the area around the baffles, these areas are divided into three regions (I, II, III). The interception performance of the different baffles is evaluated by calculating the particle mass in the three regions. Figure 9b–d illustrates the mass distribution of rock avalanche in three regions. Under MGB interception, rock avalanches showed a greater mass distribution in region I and region II. This phenomenon was particularly pronounced under M4 condition. Under the interception of SMGB and CMGB, the mass of M4 in region I and region II exceeded 400 g, surpassing the mass observed with STB and CTB. In contrast, region III exhibited the opposite phenomenon. Under the same particle condition, when the rock avalanche was intercepted by SMGB, CMGB, and TMGB, the mass distribution in region III was lower compared to STB, CTB, and TTB, respectively. The SMGB demonstrated the best interception performance, especially against the M4. Under SMGB interception, M4 had the lowest deposition mass in region III, which was only 196.8 g. Under the interception of STB, CTB, CMGB, TTB, and TMGB, the deposition mass of M4 in region III was 279.3, 549.4, 489.3, 714.7, and 413.4 g. Therefore, the interception performance of SMGB was improved by 1.42, 3.02, 2.48, 3.63, and 2.1 times compared to STB, CTB, CMGB, TTB, and TMGB, respectively.

The particle mass distribution in region III indicates the severity of the rock avalanche hazard. Lots of particles in region III suggest that more rock avalanche particles have not been intercepted, posing a threat to personnel and facilities within the protected area. When intercepted by SMGB, CMGB, and TMGB, the rock avalanche exhibits a lower mass in region III, thereby reducing the threat to the protected area.

In addition, the mass distribution of rock avalanches with different particle size within the same region varies greatly within the same region. For example, in region I, M1 was only about 113 g under SMGB blocking, while M4 was more than 480 g, which was more than 4 times. Therefore, particle size has an important influence on the distribution of rock avalanches.

3.3. Influence of Baffle Type on Rock Avalanches Impact Force. The capacity to dissipate impact force is a crucial factor in assessing baffle performance [11]. As shown in Supporting Information: Figure A3, retaining walls are placed in the areas before and after the baffles. The retaining wall is regarded as a rigid body material, and the impact force on the retaining wall is measured to indirectly reflect the ability of the baffle to dissipate the impact force of the rock avalanche particles. To evaluate different baffles more intuitively, the impact force dissipation rate η is defined as follows:

$$\eta = \frac{F_0 - F_n}{F_0} \times 100\%, \tag{11}$$

where F_0 is the impact force of rock avalanche particles on the retaining wall before the first row of baffles. F_n is the impact force on the retaining wall after the nth row of baffles, where $n = 1,2,3$.

As shown in Figure 10, the impact force dissipation rates of M1, M2, M3, and M4 rock avalanche particles against different baffles were compared.

For M1 particles (Figure 10a), TMGB displayed high impact force dissipation efficiency at the first row of baffles, with a rate of 67.7%. By the second row, the impact dissipation efficiency of SMGB, CMGB, and TMGB against rock avalanches exceeded 90%. At the third row of baffles, the dissipation rates for all types of baffles surpassed 90%. For M2 particles (Figure 10b), SMGB displayed high impact force dissipation efficiency at the first row of baffles, with a rate of 82.1%. By the second row, the impact dissipation efficiency of SMGB and CMGB against rock avalanches exceeded 95%. For M3 particles (Figure 10c), SMGB and TMGB displayed high initial dissipation efficiency at the first row of baffles, with rates of 63.93% and 76.59%, respectively, while CTB was only at 24.75%. By the second row, the efficiency of STB and SMGB significantly improved, exceeding 92%. At the third row of baffles, the dissipation rates for all types of baffles surpassed

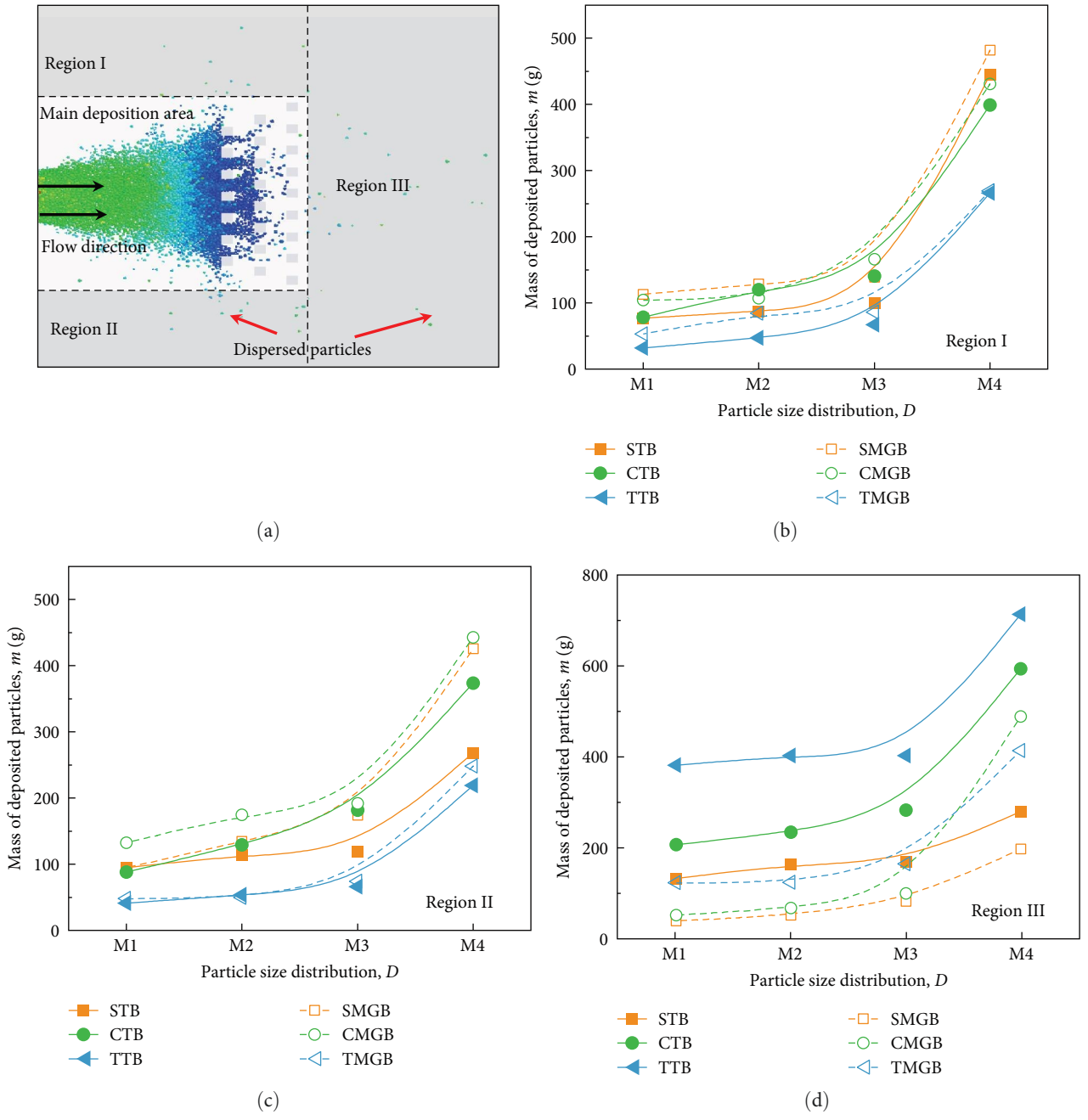

FIGURE 9: Particle mass distribution outside the main deposition region: (a) region distribution, (b) region I, (c) region II, and (d) region III.

95%. For M4 particles (Figure 10d), SMGB, CTB, and CMGB showed exceptional efficiency at the first row, with rates of 96.88%, 94.80%, and 99.88%, respectively. In contrast, STB and TTB were relatively lower, at 44.37% and 9.51%, respectively. In the second row, except for TTB and STB, the dissipation rates approached 100%, indicating increased effectiveness after successive interceptions. By the third row, nearly all the baffles reached dissipation rates close to 100%, suggesting a substantial reduction in impact force.

Overall, as particles pass through more baffles, all baffle types effectively increase the dissipation of impact force. SMGB and TMGB maintain high dissipation rates throughout the process, reflecting their consistent and efficient design in impact force reduction. Even baffles with lower initial efficiency, such as CTB, show a significant increase in dissipation rate after particles pass through multiple rows, demonstrating that a multilayered baffle setup remains effective even when initial performance is not high.

3.4. Influence of Baffle Type on Rock Avalanches Kinetic Energy. To investigate the effect of different baffles on the energy dissipation of rock avalanches, this study measured the kinetic energy (E_k) changes of rock avalanche particles of sizes M1–M4 during their impact on various baffles. The E_k

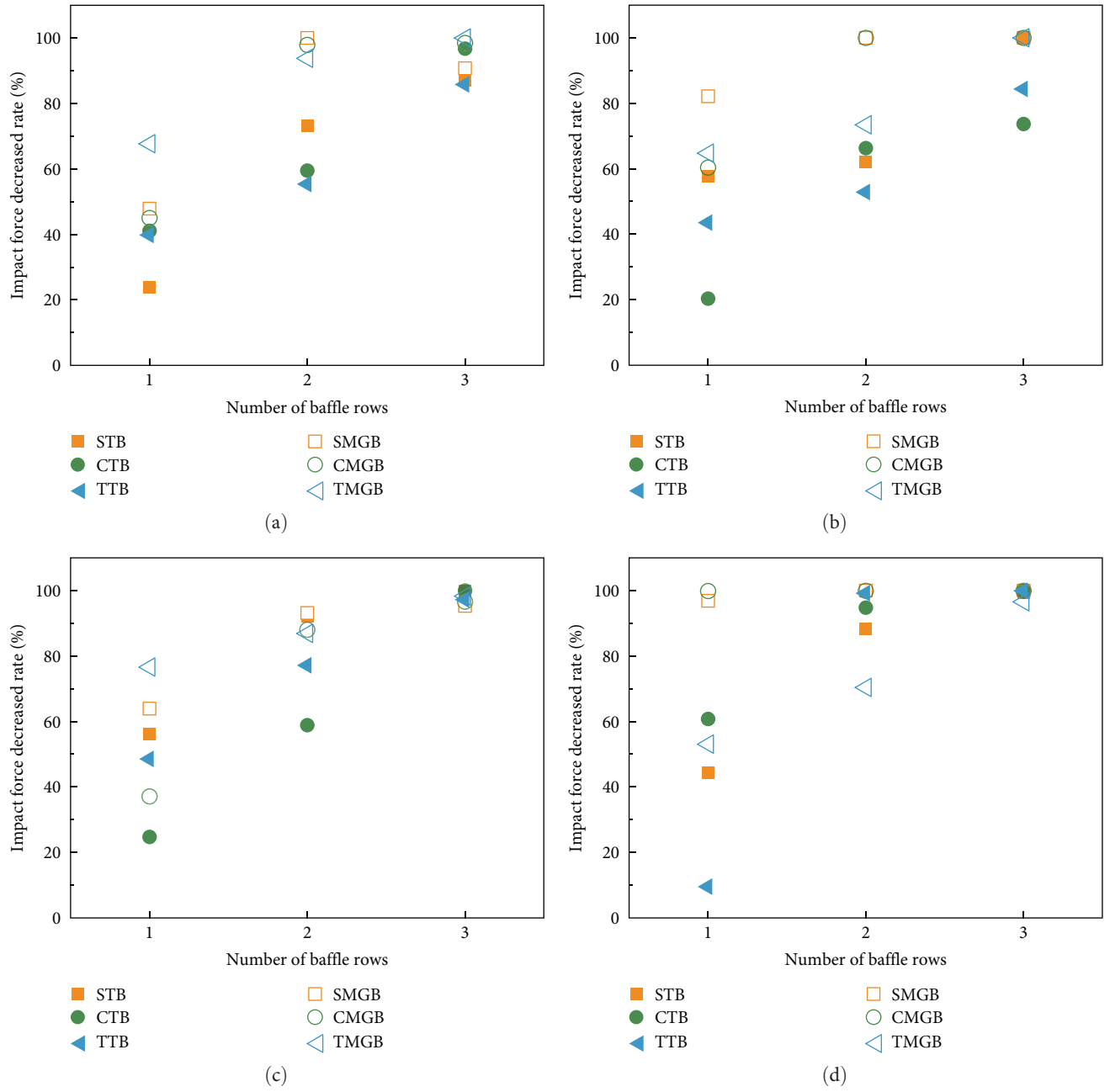

FIGURE 10: The performance of baffle type to dissipate impact force: (a) M1, (b) M2, (c) M3, and (d) M4.

was measured from the start of the particle movement until their final static deposition, with a significant time frame of $t = 1.2$–2.0 s selected for the analysis, as depicted in Figure 11. Prior to $t = 1.2$ s, the particles accelerated downhill under the influence of gravity, leading to an increase in kinetic energy. After $t = 1.2$ s, as the particles impacted the platform, the ongoing propulsion of the particles from behind kept the kinetic energy on an upward trend until $t = 1.6$ s, at which point all particle sizes, except for the largest (M4), reached their maximum kinetic energy. After $t = 1.6$ s, the particles began to decelerate due to friction and interception by the baffles, causing the kinetic energy to gradually reduce to zero. Figure 11 reveals that under the interception of six different baffles, the peak kinetic energy of rock avalanche particles follows the order M1 < M2 < M3 < M4. The larger particles (M4), possessing higher potential energy, achieve higher velocities during the acceleration phase, but due to poorer flow ability, the peak kinetic energy occurs later ($t = 1.7$ s). Additionally, the peak kinetic energy of particles impacted by MGB baffles is generally lower than those impacted by TB, with a reduction of approximately 1%–3% for the same particle size.

In conclusion, particle size directly affects the kinetic energy changes of rock avalanche particles, with larger particles exhibiting higher peak energies, posing greater demands on the design of baffles. Although MGB shows some effectiveness in reducing peak kinetic energy, the difference is not significant

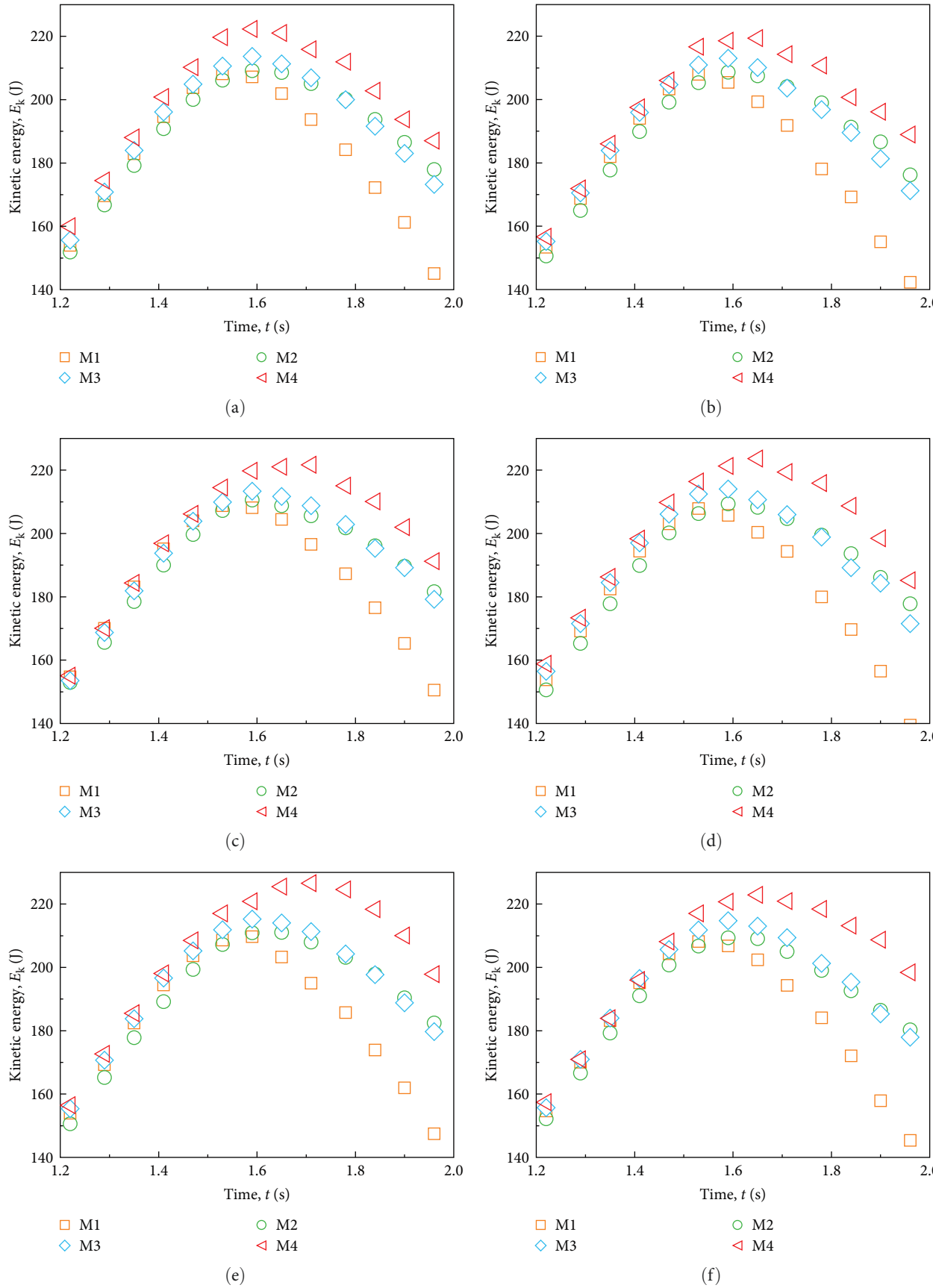

FIGURE 11: Kinetic energy of rock avalanches for different baffles: (a) STB, (b) SMGB, (c) CTB, (d) CMGB, (e) TTB, and (f) TMGB.

compared to TB, indicating room for improvement in baffle design to enhance energy dissipation capability.

4. Discussion

4.1. Analysis of Rock Avalanches Movement Characteristics With Different Baffles. Baffle structure is a "deceleration zone" built between the rock avalanches and the affected body, which can effectively restrain the moving distance and velocity of rock avalanches and reduce the kinetic energy of the flow to achieve the purpose of protecting the affected areas. However, the structures of arrays of baffle in previous studies were mostly square, and research showed that the shape of baffles had a great impact on their performance [24]. Wang et al. [15] and Wang et al. [46] analyzed the performance of ASBs, CB, and SB, and found that with the same parameter, the arc-shaped structures perform better than CB and SB on the blockage ratio, deposition area, and energy consumption on rock avalanches. In order to better compare the performance of different arrays of baffle, the velocity reduction ratio (VRR) is defined as v as follows:

$$v = \frac{V_0 - V_b}{V_0} \times 100\%, \tag{12}$$

where V_0 is the velocity of rock avalanches before passing through the first row of baffles, V_b is the velocity of rock avalanches after passing through baffle.

The blocking ratio (BR) is defined as n as follows:

$$n = \frac{m_t - m_b}{m_t} \times 100\%, \tag{13}$$

where m_t is the total mass of rock avalanche particles, m_b is the particle mass after the baffle.

The impact force dissipation ratio (IFDR) is Equation (11), where the value of n is taken as 3.

The energy dissipation ratio (EDR) is defined as ε as follows:

$$\varepsilon = \frac{E_0 - E_b}{E_0} \times 100\%, \tag{14}$$

where E_0 is the maximum kinetic energy of rock avalanches before passing through the first row of baffles, E_b is the maximum kinetic energy of rock avalanches after passing through baffles.

Figure 12 analyzes the characteristics of the movement of the rock avalanches with different baffle structures, triangular baffle [22], SB, ASB [46]. As shown in Figure 12, the VRR of different baffles for rock avalanches was compared. The VRRs of SB, TB, ASB, and SMGB were 0.27, 0.19, 0.26, and 0.45, respectively. About BR, TB, ASB, and SMGB had higher blockage ratios, all above 85%, which enabled them to intercept more particles, but also more likely to cause particle deposition. However, the BR of TTB was only 18.84%, and the reason for the large difference was the location. Huang et al. [22] placed TTB on the chute, and the inertia and the gravity of rock avalanche particles made it easier to pass through the gaps

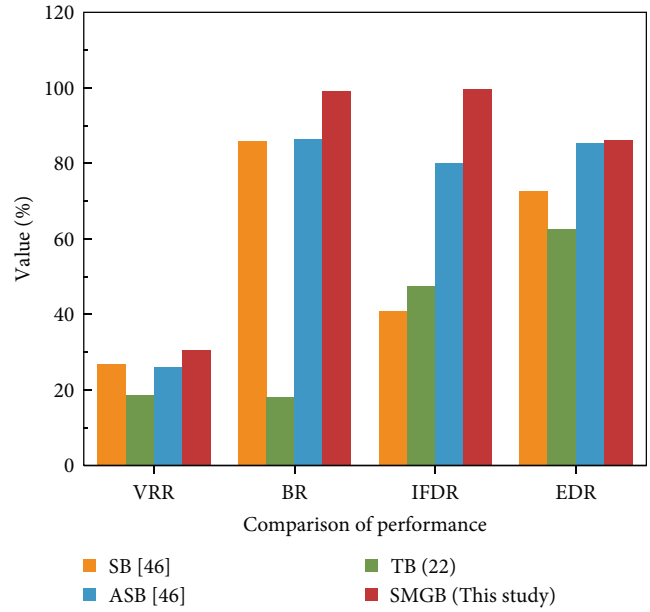

FIGURE 12: Analysis of rock avalanches movement characteristics of different baffles.

between the arrays of baffle. The IFDR of different arrays of baffle is shown in Figure 12. In terms of the IFDR, SMGB > ASB > TTB > TB, and the IFDR were 91.6%, 47.5%, 92%, and 99.6%, respectively. It was noted that the IFDR of TTB here was greater than that of TB, which was different from the results of this study, and its reason was also related to the location. The TTB placed at the chute could disturb the flow condition of random rock avalanches to a greater extent, and further reduce the impact force compared to TB, which was placed on the platform. Finally, the EDR of different baffles for rock avalanches was compared. Four baffles had good effects on the kinetic energy consumption of rock avalanches, and SMGB and ASB had better energy consumption effects, both reaching more than 80%. Due to the great differences in the actual settings and research conditions of the arrays of baffle, the comparison indicators used are dimensionless, so the indicators can only preliminarily validate the superiority of MGB in rock avalanche prevention.

4.2. The Mechanism of Rock Avalanches–MGB Interaction. Figure 13 analyzes the mechanism of particle interception and energy dissipation capability of the MGB. When rock avalanche particles impacted the baffles, they interacted with both the main structure and the prop root structure (Figure 13a,b). The main structure was similar to STB, dissipating the velocity of the rock avalanches during this interaction (Figure 13c1). As shown in Figure 13c2, the rock avalanche interacted with the baffle, where part of the kinetic energy was absorbed by the main structure, while the remaining energy was absorbed by the prop root. In addition, particle-to-particle collisions further dissipated kinetic energy. When rock avalanche particles hit the prop root structure, larger particles were intercepted by the prop roots and could not pass through the gaps between the baffles. This caused particle blockage,

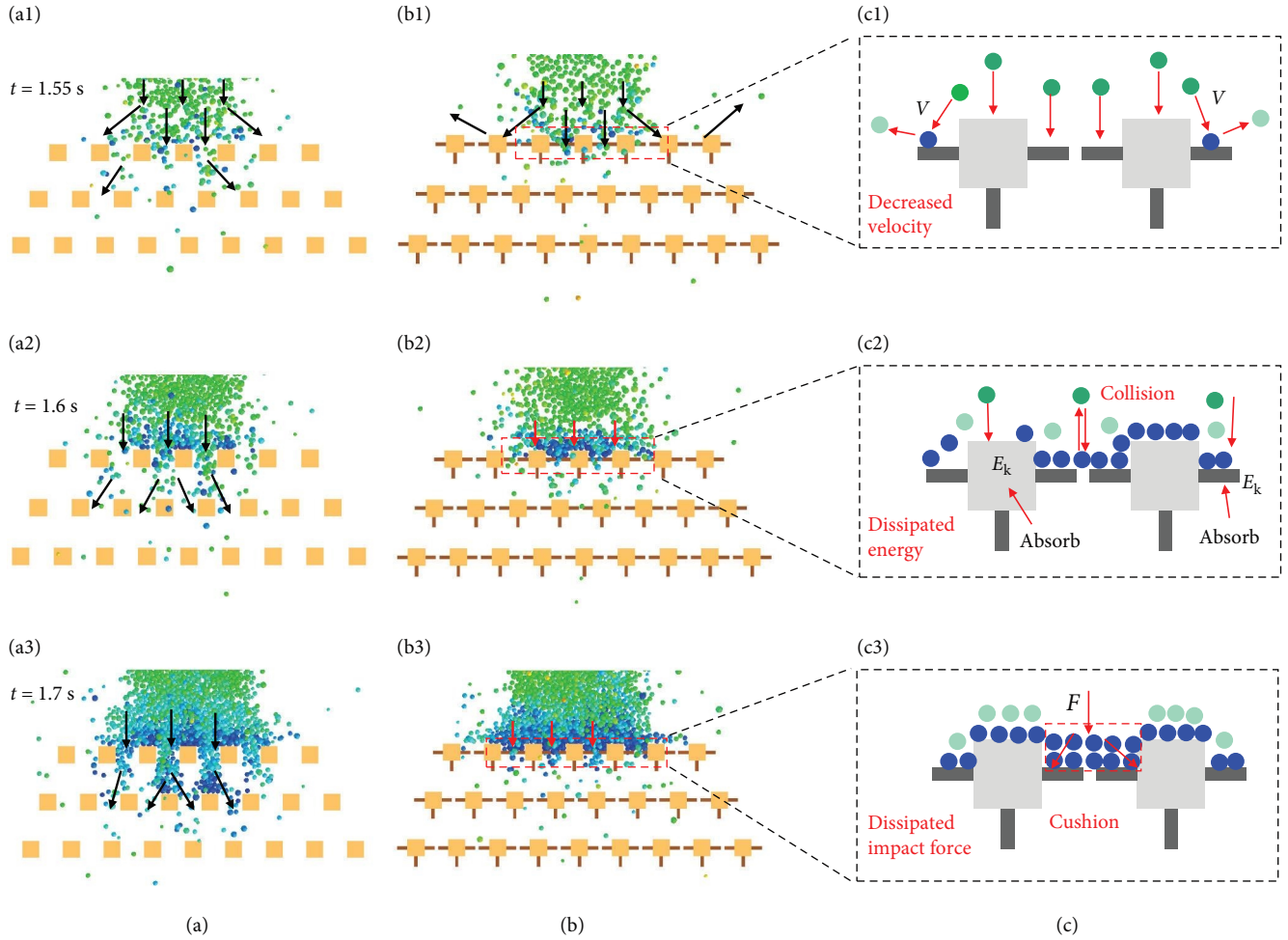

FIGURE 13: Protection mechanism of MGB: (a; a1–a3) the process of interactions between rock avalanche and baffle; (b; b1–b3) the process of interactions between rock avalanche and SMGB; and (c; c1–c3) the mechanism of velocity decrease, energy dissipation, and impact force dissipation.

forming a buffer cushion that decreases impact force of subsequent rock avalanche particles (Figure 13c3).

Supporting Information: Figure A4a,b illustrates the particle segregation and climbing behavior of rock avalanche particles (M1–M4) after interacting with SBs. From the final deposition state, it was evident that particle segregation was closely related to particle size configuration. During moving, smaller particles, due to their lower mass and higher energy, tended to migrate to the lower layers, while larger particles, with greater inertia, remained in the upper layers. This particle segregation effect led to a gradual increase in the overall climbing height of the rock avalanches. Figure 14a quantitatively compared the final climbing height of different rock avalanche particles, showing that the climbing height under the SMGB was generally higher than that under the MGB. Under the SMGB, the climbing height increased with particle size, with M1–M4 particles reaching climbing heights of 81, 97, 115, and 138 mm, respectively. In contrast, under the STB, although the overall climbing height was lower than that under the SMGB, it still showed an increasing trend with particle size, with M1–M4 particles reaching heights of 77, 96, 110, and 120 mm, respectively. It was noteworthy that when interacting with the second and third rows of baffles, the climbing height of rock avalanches exhibited an opposite trend.

Figure 14b shows the dynamic process of particle segregation and climbing for the rock avalanches. Figure 14 b1 illustrates the climbing process of particle flow along the baffles, where larger particles, due to their higher kinetic energy, reached greater height during movement. Figure 14b2 depicts the particle segregation process, where smaller particles, due to their better flow ability, concentrated more at the lower levels, while larger particles were gradually pushed to the top by the underlying smaller particles, further increasing the overall climbing height. Finally, Figure 14b3 shows the state of particles gradually coming to rest, with a clear stratification phenomenon, smaller particles increased in proportion from top to bottom, while the proportion of larger particles decreased, demonstrating a significant particle segregation characteristic.

4.3. The Economic Benefits of Different Baffles Against Rock Avalanches. Different shapes of baffles were used in this study. Due to the difference in shape, the volume of each type of baffle is different, so the cost is also different. In this study, the height of each baffle is 18 cm. The base length of the SB is 5 cm, the

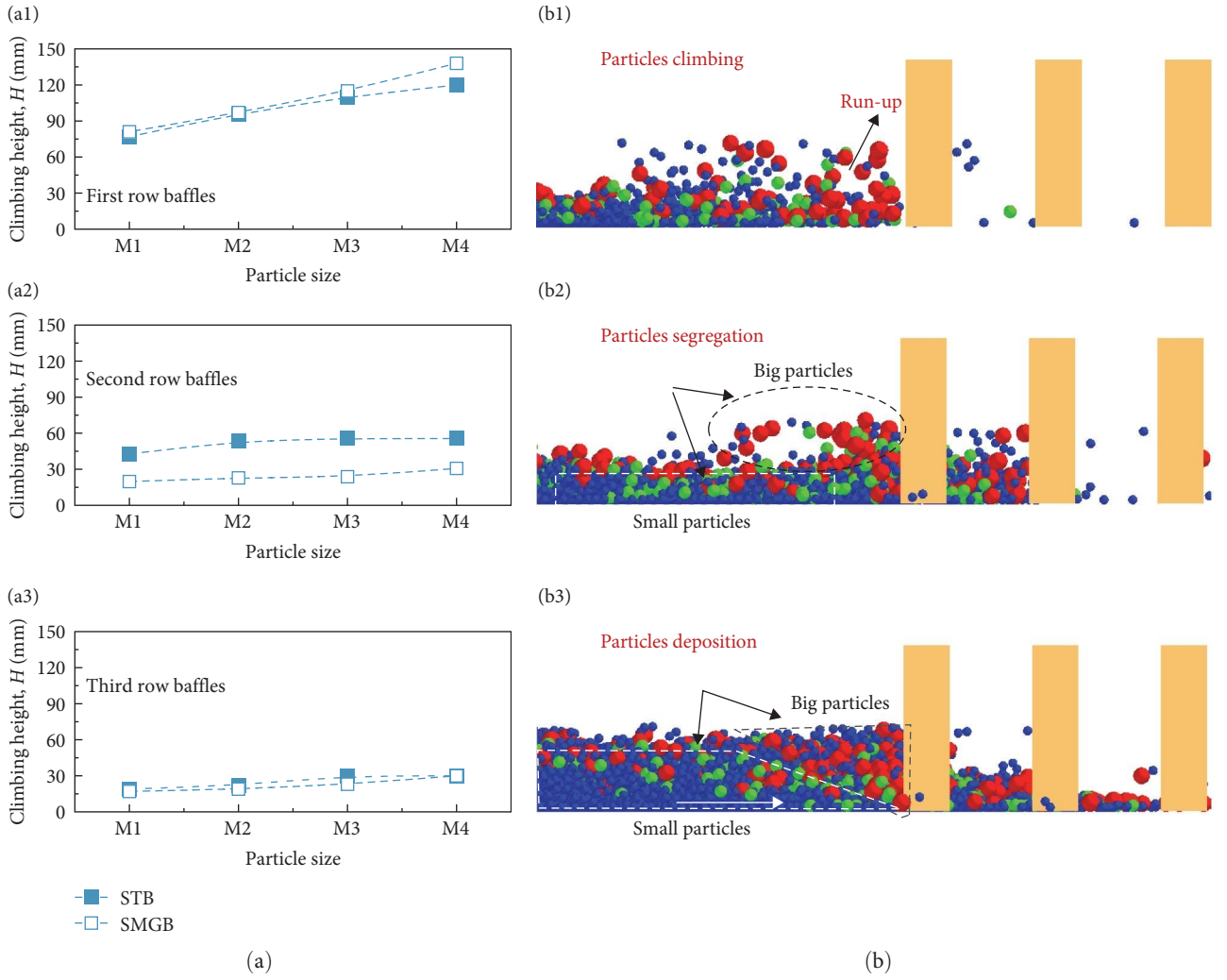

FIGURE 14: Particles climbing mechanism: (a; a1–a3) climbing height analysis and (b; b1–b3) dynamic climbing process of rock avalanches particles.

diameter of the cylindrical baffle is 5 cm, and the side length of the triangular baffle is 7.5 cm. Based on the physical model experiment and the geometric similarity to actual working conditions, we estimated the concrete volume and cost required for the baffles. These estimates were made using the model size of the six baffle types (Supporting Information: Table A3).

In order to analyze the economic benefits of different baffles, we introduced a cost–benefit ratio (CBR). CBR is a crucial economic indicator used to measure the economic benefits of a project or measure, indicating the benefits brought by the unit cost. In this study, the direct economic loss caused by the rock avalanche is assumed to be 1 million dollars, and the benefit represents the economic loss recovered. The benefit value is calculated as the product of the direct economic loss and the baffle protection effectiveness (refer to Section 3.3). The cost represents the material cost of the baffles. The CBR curves for each baffle type are shown in Supporting Information: Figure A5. Under the impact of M1–M4, the baffles with the highest CBR are CTB (111.64), SMGB (155.87), SMGB (121.34), and CMGB (234.35), respectively. Almost all baffles showed a decreasing CBR with an increasing number of baffle rows, indicating that increasing the number of baffle rows will increase the cost, but the improvement of protection effect was not significant. Although the CBR decreased with the increase in the number of baffle rows, its values were all greater than 1, indicating that there was still a benefit. Furthermore, from a safety perspective, a single row of baffles is insufficient to intercept all rock avalanches. Therefore, on the whole, the two rows of baffles are a more reasonable arrangement, which not only meets the protection requirements but also controls the cost. Therefore, overall, two rows of baffles are considered a reasonable arrangement, achieving the required protection while controlling cost.

In addition, material selection plays a crucial role in both the cost and sustainability of protective structures. While TBs use reinforced concrete or steel, alternative materials have been explored to enhance sustainability and cost efficiency [47]. The use of environmentally friendly or recycled materials in

engineering could offer promising solutions for improving the economic feasibility of protective structures against rock avalanches.

5. Conclusion

Baffle structures are effective measures against rock avalanche hazards. Building upon TB designs, this study proposed a new mangrove-guarded baffle based on the structure of mangrove roots. Using EDEM software, the study simulated flume rock avalanches and obtained a series of input parameters by similarly comparing with physical models in terms of deposition and velocity changes. After calibrating these parameters, the research explored the impacts of baffle type and particle size on the movement velocity, deposition morphology, impact force, and kinetic energy changes of rock avalanche particles. The following conclusions could be drawn from this study:

1. The process of rock avalanche particles impacting baffles was divided into four stages: initiation, acceleration, impact, and static deposition. The size of the particles determined the evolution of the velocity. With the increase in the size of the rock avalanche particles, their frontal and tail velocity increased, which was due to the decrease in the friction between the particles.
2. Under the CMGB, the volume of the dead zone produced was the largest. The dead zone volume of M1–M4 accounted for 5.08%, 7.0%, 6.44%, and 7.49% of the total volume, respectively. Compared to the STB, under the SMGB, the deposition areas of M1–M4 decreased by 17.9%,12.7%,17.1%, and 16%, respectively. The MGB effectively retained the particles and restricted its movement through prop roots.
3. Multirowed baffle configurations significantly enhanced impact force dissipation in rock avalanches. The SMGB and TMGB baffles demonstrated superior impact force dissipation, with SMGB achieving up to 99.88% efficiency for M4 particles by the third row, highlighting its advantage in dissipating the energy of rock avalanches.
4. MGB had some effectiveness in dissipating the energy of rock avalanche particles, but the effect was not significant compared to TB, reducing the dynamic energy of the rock avalanche flow by only 1%–3%. Therefore, the kinetic energy of cuttings is mainly affected by the size of particle size.
5. The protection mechanism of the MGB was realized through three aspects: the main structure and the prop roots structure jointly reduced the velocity, absorbed energy, and dissipated the impact force of the rock avalanche. In the actual project, considering the economic benefits and protection performance, the arrangement of two rows of baffles could be the best solution.

Data Availability Statement

The data that support the findings of this study are available from the first author, Xin-Po Sun, upon reasonable request.

Ethics Statement

Not applicable for studies not involving humans or animals.

Disclosure

All authors have read and agreed to the published version of the manuscript. The authors agree to publication in the journal indicated below and also to publication of the article in English by Wiley's corresponding English-language journal.

Conflicts of Interest

The authors declare no conflicts of interest.

Author Contributions

Xin-Po Sun: writing – review and editing, writing – original draft, resources, methodology, funding acquisition. **Shi-Jie Luo**: writing – review and editing, writing – original draft, investigation, software, validation. **Chun-Ying Wang**: writing – review and editing, investigation, data curation, validation, formal analysis. **Lu Zheng**: visualization, methodology, investigation. **Wan-Hui Su**: visualization, data curation. **Xin-Yi Wang**: supervision, project administration, conceptualization, formal analysis. **Zhe-Yuan Jiang**: writing – review and editing, validation, supervision, project administration, conceptualization. Xin-Po Sun, Shi-Jie Luo, and Chun-Ying Wang contributed equally to this work and are co-first authors of this manuscript.

Funding

This study was financially supported by the Youth Innovation Promotion Association of the Chinese Academy of Sciences (Grant 2021373), the Key Projects of Science and Technology Department of Sichuan Province (Grant 2020YJ0360), the Sichuan Education and Teaching Reform Project (Grant JG2021-1070), and the Opening Project of Sichuan Province University Key Laboratory (Grant SC_FQWLY-2020-Z-02).

Acknowledgments

The authors sincerely thank Yuzhang BI for his constructive suggestions on manuscript writing and revision. During the writing process, the authors used ChatGPT, a product of OpenAI, for partial translation and language polishing, specifically for the abstract and some sections of the data analysis.

Supporting Information

Additional supporting information can be found online in the Supporting Information section. (*Supporting Information*)
The Supporting Information primarily encompass detailed information for all authors, supporting figures (Figures A1–A5), and supporting tables (Tables A1–A3).

References

[1] O. Hungr, S. Leroueil, and L. Picarelli, "Picarelli L the Varnes Classification of Landslide Types, an Update," *Landslides* 11, no. 2 (2014): 167–194.

[2] A. Strom, "Rock Avalanches: Basic Characteristics and Classification Criteria," in *Understanding and Reducing Landslide Disaster Risk*, eds. V. Vilímek, F. Wang, A. Strom, K. Sassa, P. T. Bobrowsky, and K. Takara, 5, (Springer, Cham, 2021): 3–23.
[3] H. X. Lan, Y. X. Zhang, R. Macciotta, et al., "The Role of Discontinuities in the Susceptibility, Development, and Runout of Rock Avalanches: A Review," *Landslides* 19, no. 6 (2022): 1391–1404.
[4] M. Geertsema and A. Bevington, "A Cautionary Note for Rock Avalanche Field Investigation: Recent Sequential and Overlapping Landslides in British Columbia," *Canadian Geotechnical Journal* 58, no. 5 (2021): 737–740.
[5] Y. Zhuang, Q. Xu, and A. Xing, "Numerical Investigation of the Air Blast Generated by the Wenjia Valley Rock Avalanche in Mianzhu, Sichuan, China," *Landslides* 16, no. 12 (2019): 2499–2508.
[6] M. Zhang and Y. Yin, "Dynamics Mobility-Controlling Factors and Transport Mechanisms of Rapid Long-Runout Rock Avalanches in China," *Engineering Geology* 167, no. 167 (2013): 37–58.
[7] A. Remaître, T. W. J. van Asch, J.-P. Malet, and O. Maquaire, "Influence of Check Dams on Debris-Flow Run-Out Intensity," *Natural Hazards and Earth System Sciences* 8, no. 6 (2008): 1403–1416.
[8] S. Li, Y. You, X. Chen, J. Liu, and J. Chen, "Regulation Effectiveness of a Window-Check Dam on Debris Flows," *Engineering Geology* 253, no. 253 (2019): 205–213.
[9] A. M. Ferrero, A. Segalini, and G. Umili, "Experimental Tests for the Application of an Analytical Model for Flexible Debris Flow Barrier Design," *Engineering Geology* 185, no. 185 (2015): 33–42.
[10] A. Leonardi, S. R. Goodwin, and M. Pirulli, "The Force Exerted by Granular Flows on Slit Dams," *Acta Geotechnica* 14, no. 6 (2019): 1949–1963.
[11] C. W. W. Ng, C. E. Choi, D. Song, et al., "Physical Modeling of Baffles Influence on Landslide Debris Mobility," *Landslides* 12, no. 1 (2015): 1–18.
[12] S. R. Goodwin, C. E. Choi, and C.-Y. Yune, "Towards Rational use of Baffle Arrays on Sloped and Horizontal Terrain for Filtering Boulders," *Canadian Geotechnical Journal* 58, no. 10 (2021): 1571–1589.
[13] D. Song, C. E. Choi, C. W. W. Ng, and G. G. D. Zhou, "Geophysical Flows Impacting a Flexible Barrier: Effects of Solid-Fluid Interaction," *Landslides* 15, no. 1 (2018): 99–110.
[14] C. E. Choi, C. W. W. Ng, D. Song, et al., "Flume Invest Igation of Landslide Debris–Resisting Baffles," *Canadian Geotechnical Journal* 51, no. 5 (2014): 540–553.
[15] D. Wang, Q. Li, Y. Bi, and S. He, "Effects of New Baffles System Under the Impact of Rock Avalanches," *Engineering Geology* 264, no. 264 (2020): 105261.
[16] C. W. W. Ng, C. E. Choi, R. C. H. Koo, et al., "Dry Granular Flow Interaction With Dual-Barrier Systems," *Géotechnique* 68, no. 5 (2018): 386–399.
[17] Y. Z. Bi, X. P. Sun, H. Z. Zhao, et al., "Comparison Regarding the Effects of Different Baffle Systems as Impacted by Rock Avalanches," *International Journal of Civil Engineering* 19, no. 2 (2021): 127–144.
[18] C. Scheidl, C. Friedl, L. Reider, et al., "Impact Dynamics of Granular Debris Flows Based on a Small-Scale Physical Model," *Acta Geotechnica* 19 (2023): 3979–3997.
[19] C. E. Choi, C. W. W. Ng, R. P. H. Law, D. Song, J. S. H. Kwan, and K. K. S. Ho, "Computational Investigation of Baffle Configuration on Impedance of Channelized Debris Flow," *Canadian Geotechnical Journal* 52, no. 2 (2015): 182–197.
[20] R. P. H. Law, C. E. Choi, and C. W. W. Ng, "Discrete-Element Investigation of Influence of Granular Debris Flow Baffles on Rigid Barrier Impact," *Canadian Geotechnical Journal* 53, no. 1 (2016): 179–185.
[21] Y.-Z. Bi, S.-M. He, X.-P. Li, et al., "Geo-Engineered Buffer Capacity of Two-Layered Absorbing System Under the Impact of Rock Avalanches Based on Discrete Element Method," *Journal of Mountain Science* 13, no. 5 (2016): 917–929.
[22] Y. Huang, B. Zhang, and C. Zhu, "Computational Assessment of Baffle Performance Against Rapid Granular Flows," *Landslides* 18, no. 1 (2021): 485–501.
[23] Y.-Z. Bi, D.-P. Wang, S.-X. Yan, Q.-Z. Li, and S.-M. He, "Research on the Blocking Effect of Baffle-Net Structure on Rock Avalanches: Consider the Influence of Particle Splashing," *Bulletin of Engineering Geology and the Environment* 82, no. 7 (2023): 277.
[24] C. E. Choi, Y. Cui, L. H. D. Liu, C. W. W. Ng, and S. D. N. Lourenço, "Impact Mechanisms of Granular Flow Against Curved Barriers," *Géotechnique Letters* 7, no. 4 (2017): 330–338.
[25] Y.-Z. Bi, X.-Y. Wang, D.-P. Wang, Z.-F. Li, M. Lovati, and B. Zhang, "A Methodological Study on the Design Defending Baffles Based on Mangrove Bionics," *Buildings* 13, no. 2 (2023): 310.
[26] Y. Cui, C. E. Choi, L. H. D. Liu, and C. W. W. Ng, "Effects of Particle Size of Mono-Disperse Granular Flows Impacting a Rigid Barrier," *Natural Hazards* 91, no. 3 (2018): 1179–1201.
[27] Y.-J. Jiang, X.-Y. Fan, T.-H. Li, and S.-Y. Xiao, "Influence of Particle-Size Segregation on the Impact of Dry Granular Flow," *Powder Technology* 340, no. 340 (2018): 39–51.
[28] N. Sanvitale and E. T. Bowman, "Visualization of Dominant Stress-Transfer Mechanisms in Experimental Debris Flows of Different Particle-Size Distribution," *Canadian Geotechnical Journal* 54, no. 2 (2017): 258–269.
[29] M. A. Cabrera and W. Wu, "Experimental Modelling of Free-Surface Dry Granular Flows Under a Centrifugal Acceleration Field," *Granular Matter* 19, no. 4 (2017): 78.
[30] J. M. N. T. Gray, "Particle Segregation in Dense Granular Flows," *Annual Review of Fluid Mechanics* 50, no. 1 (2018): 407–433.
[31] J.-Y. Nie, Y. Cui, Z. Wu, L. Zhang, and J. Fang, "DEM Study on Role of Fines in Mobility of Dry Granular Flows Considering Particle Size-Shape Correlation," *Computers and Geotechnics* 166 (2024): 105980.
[32] W. Li, S. Yan, D. Wang, et al., "A Semi-Empirical Impact Force Model of Irregular Rockfall on Granular Layer and Its Experimental Validation," *Acta Geotechnica* 19, no. 4 (2024): 2213–2231.
[33] C. Wang, Y. Cui, D. Song, J. Nie, and B. Hu, "Effect of Ice Content on the Interaction Between Rock–Ice Avalanche and Rigid Barrier: Physical and Numerical Modelling," *Computers and Geotechnics* 150 (2022): 104924.
[34] J. Fang, Y. Cui, X. Li, and J. Nie, "A New Insight Into the Dynamic Impact Between Geophysical Flow and Rigid Barrier," *Computers and Geotechnics* 148 (2022): 104790.
[35] G. G. D. Zhou, J. Du, D. Song, C. E. Choi, H. S. Hu, and C. Jiang, "Numerical Study of Granular Debris Flow Run-up Against Slit Dams by Discrete Element Method," *Landslides* 17, no. 3 (2020): 585–595.
[36] H. Teufelsbauer, Y. Wang, S. P. Pudasaini, R. I. Borja, and W. Wu, "DEM Simulation of Impact Force Exerted by Granular Flow on Rigid Structures," *Acta Geotechnica* 6, no. 3 (2011): 119–133.

[37] B. Zhang and Y. Huang, "Effect of Unsteady Flow Dynamics on the Impact of Monodisperse and Bidisperse Granular Flow," *Bulletin of Engineering Geology and the Environment* 81, no. 2 (2022): 77.
[38] S. B. Savage and K. Hutter, "The Motion of a Finite Mass of Granular Material Down a Rough Incline," *Journal of Fluid Mechanics* 199 (1989): 177–215.
[39] S. B. Savage and K. Hutter, "The Dynamics of Avalanches of Granular Materials From Initiation to Runout. Part I: Analysis," *Acta Mechanica* 86, no. 1–4 (1991): 201–223.
[40] P. A. Cundall and O. D. L. Strack, "A Discrete Numerical Model for Granular Assemblies," *Géotechnique* 29, no. 1 (1979): 47–65.
[41] T. Pöschel and T. Schwager, *Computational Granular Dynamics: Models and Algorithms* (Springer Science & Business Media, 2005).
[42] J. Ellowitz, H. Turlier, N. Guttenberg, W. W. Zhang, and S. R. Nagel, "Still Water: Dead Zones and Collimated Ejecta From the Impact of Granular Jets," *Physical Review Letters* 111, no. 16 (2013): 168001.
[43] T. Faug, "Depth-Averaged Analytic Solutions for Free-Surface Granular Flows Impacting Rigid Walls Down Inclines," *Physical Review E* 92, no. 6 (2015): 062310.
[44] O. Pouliquen and Y. Forterre, "Friction Law for Dense Granular Flows: Application to the Motion of a Mass Down a Rough Inclined Plane," *Journal of Fluid Mechanics* 453 (2002): 133–151.
[45] P. Jop, Y. Forterre, and O. Pouliquen, "A Constitutive Law for Dense Granular Flows," *Nature* 441, no. 7094 (2006): 727–730.
[46] D. Wang, Y. Bi, Q. Li, and S. He, "Kinetic Response Analysis of Different Types of Baffle Submitted to Rock Avalanches Based on Discrete Element Method," *Environmental Earth Sciences* 80, no. 17 (2021): 600.
[47] Z.-Y. Jiang, X.-P. Sun, Y.-Q. Luo, X.-L. Fu, A. Xu, and Y.-Z. Bi, "Recycling, Reusing and Environmental Safety of Industrial by-Product Gypsum in Construction and Building Materials," *Construction and Building Materials* 432, no. 432 (2024): 136609.